

Mechanism of CO Displacement from an Unusually Labile Rhenium Complex: An Experimental and Theoretical Investigation

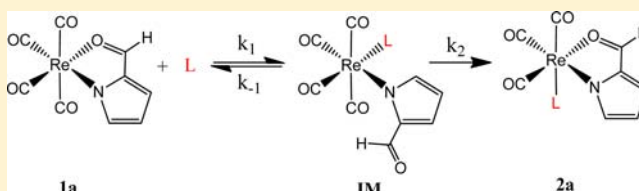
Sohail Muhammad,[†] Veeranna Yempally,[†] Muhammad Anas,[†] Salvador Moncho,[†] Samuel J. Kyran,[‡] Edward N. Brothers,[†] Donald J. Darensbourg,^{*,‡} and Ashfaq A. Bengali^{*,†}

[†]Department of Chemistry, Texas A&M University at Qatar, Doha, Qatar

[‡]Department of Chemistry, Texas A&M University, College Station, Texas 77843, United States

Supporting Information

ABSTRACT: The displacement of a CO ligand from an unusually labile rhenium carbonyl complex containing a bidentate carboxyaldehyde pyrrolyl ligand by PPh₃ and pyridine has been investigated. The reaction is found to proceed by an associative, preequilibrium mechanism. Theoretical calculations support the experimental data and provide a complete energetic profile for the reaction. While the Re–CO bond is found to be intrinsically weak in these complexes, it is postulated that the unusual lability of this species is due to the presence of a weak aldehyde Re–O link that can easily dissociate to open a coordination site on the metal center and accommodate an incoming ligand prior to CO loss. The resulting intermediate complex has been identified by IR spectroscopy. The presence of the hemilabile pyrrolyl ligand provides a lower-energy reaction channel for the release of CO and may be of relevance in the design of CO-releasing molecules.



INTRODUCTION

While transition-metal carbonyl complexes are often used as stoichiometric or catalytic reagents for a variety of chemical transformations,¹ there is increasing interest in their utility as reagents in systems of biological relevance.² For example, new radiopharmaceuticals based on the Re(CO)₃ and Tc(CO)₃ fragments that bind to estrogen receptors have been synthesized.³ The strong IR absorption of the CO ligands also provides a useful spectroscopic tag that has led to the development of carbonylmetalloimmunoassay procedures.⁴ Some metal carbonyl complexes also show promise as anticancer drugs.⁵ Recently, CO has been identified as having an important pharmacological function and, like NO, is thought to possess vasodilatory properties.⁶ Several other beneficial physiological effects of CO have been well documented.^{2a,6a,b,d} As a result, there have been some early investigations into the use of metal carbonyl complexes as sources of solid CO and therefore as CO-releasing molecules (CORMs).^{5b,6c} For example, among other complexes, [Ru(CO)₃Cl₂]₂ and Ru(CO)₃Cl(glycinate) have been shown to readily transfer CO to myoglobin (Mb) to form Mb-CO under physiological conditions.⁷ Other CORMs demonstrate a therapeutic value in reducing sepsis-induced lethality by inhibiting bacterial growth and respiration.⁸

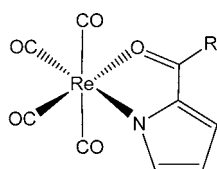
Recently, Bideau and co-workers reported the synthesis of a series of bidentate pyrrole-based rhenium tetracarbonyl complexes that have potential utility as radiopharmaceutical reagents because of the incorporation of ¹⁸⁶Re or ¹⁸⁸Re as a radionuclide (**1**).⁹ Our interest in these complexes was motivated by the reported unusual lability of the *cis*-CO ligands in the presence of donor molecules such as PPh₃.

Surprisingly, CO substitution by the weakly coordinating tetrahydrofuran solvent also occurred readily, even at room temperature. As noted by the authors, the ease of CO loss in these complexes may lead to their application as CORMs. Given this promising application, it becomes important to investigate both the mechanism and energetics of the CO loss pathway. The CO lability of **1** is in marked contrast to some other rhenium carbonyl complexes such as the thermally robust CpRe(CO)₃ molecule. An important characteristic of **1** that might assist in facile CO replacement is the presence of the presumed weak Re–O interaction. This bond could potentially be disrupted by an incoming ligand, thereby opening up a coordination site on the rhenium metal center and providing a low-energy pathway for CO loss. This process would be somewhat analogous to an associative “ring-slip” mechanism¹⁰ in the substitution of CO from molecules such as (η^5 -C₁₀H₉)Mn(CO)₃, whereby an open coordination site is generated upon an $\eta^5 \rightarrow \eta^3$ hapticity shift of the hydro-naphthalene ring system, facilitating incoming ligand binding prior to CO loss.¹¹

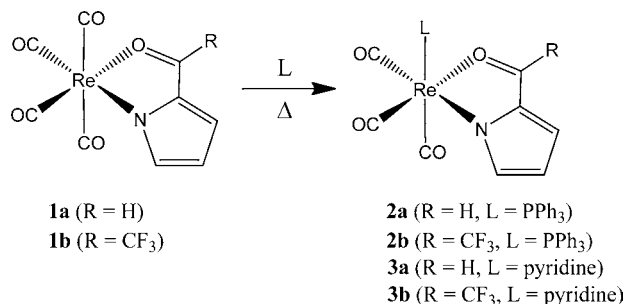
We report in this paper an experimental and theoretical study aimed at understanding the mechanism of CO displacement (Scheme 1) from **1a** and **1b** by PPh₃ and pyridine to form compounds **2a** and **2b** and compounds **3a** and **3b**, respectively. The results provide details about the energetics of this process and lead to identification of an important intermediate along the reaction pathway. Detailed calculations using density

Received: October 7, 2012

Published: November 15, 2012

1 (R = H, CH₃, CCl₃, OMe)

Scheme 1



functional theory (DFT) provide additional support for the experimental data.

EXPERIMENTAL AND THEORETICAL DETAILS

a. Kinetic Experiments. All kinetic experiments were performed with a Bruker Vertex 80 Fourier transform infrared (FTIR) spectrometer. Spectra were obtained at 4 cm⁻¹ resolution. A temperature-controlled 0.75-mm IR cell with CaF₂ windows was used to obtain all spectra. A typical kinetic run was performed as follows. An appropriate amount of PPh₃ or pyridine was added to a 3 mM heptane solution of **1a** or **1b**. A background spectrum was taken immediately, followed by the acquisition of sample spectra at defined time intervals over a 303–333 K temperature range. Observed rate constants (*k*_{obs}) were obtained from first-order fits to the temporal profile of either reactant decay or product growth. The stated errors in the rate constants and activation parameters were obtained from a least-squares fit to the data, as reported by the data analysis program *Kaleidagraph*.

b. Synthesis. The tetracarbonylrhenium complex with the 2-formylpyrrolyl ligand {2-(CHO)-C₄H₃N}Re(CO)₄ (**1a**) was prepared as per the literature.⁹ Solvents were either anhydrous grade (Aldrich) or purified by an MBraun Manual Solvent Purification System packed with an Alcoa F200 activated alumina desiccant. NMR spectra were recorded on a Varian INOVA 500 (operating at 499.42, 202.17, and 125.59 MHz for ¹H, ³¹P, and ¹³C, respectively) or a Bruker Avance II 400 spectrometer. ¹H and ¹³C NMR spectra were referenced to residual solvent resonances, while ³¹P NMR spectra were referenced to an external H₃PO₄ in D₂O at 0.0 ppm. IR spectra were obtained on a Bruker Tensor 27 or Vertex 80 FTIR spectrometer. Elemental analyses for **1b**, **2b**, and **3a** were determined by Atlantic Microlab (Norcross, GA).

Synthesis of {2-(CF₃CO)-C₄H₃N}Re(CO)₄ (1b**).** Re(CO)₅Br (0.770 g, 1.90 mmol), 2-(trifluoroacetyl)pyrrole (0.312 g, 1.91 mmol), and sodium *tert*-butoxide (0.206 g, 2.14 mmol) in toluene (25 mL) were heated to reflux for 2 h under an argon atmosphere. The resulting vermilion solution was filtered to remove NaBr and the solvent concentrated to give a viscous oil. This was purified by flash chromatography on silica (6:4 pentane/ether) to obtain a dark-orange oil (the small presence of Re₂(CO)₁₀ can be removed by a second flash chromatography with 9:1 pentane/CH₂Cl₂), which crystallizes as a dark-red solid after the complete removal of residual solvent on a rotovap (0.260 g, 30%). IR data in heptane (ν_{CO}): 1583 (m), 1958 (s), 2001 (s), 2014 (s), 2115 (m). NMR data in CDCl₃: ¹H δ 6.61 (dd, *J* = 4.6 and 1.3 Hz, 1 H), 7.46 (m, 1 H), 7.70 (m, 1 H); ¹³C{¹H} δ 117.9 (q, ¹J_{CF} = 280 Hz, 1 C, CF₃), 121.5, 128.0 (q, ⁴J_{CF} = 3 Hz, 1 C), 139.6, 151.9, 172.7 (q, ²J_{CF} = 38 Hz, 1 C, C=O), 183.6 (s, 2 C, CO), 188.3

(s, 1 C, CO), 188.5 (s, 1 C, CO). Anal. Calcd for C₁₀H₃F₃N₁O₅Re₁: C, 26.1; H, 0.7; N, 3.0. Found: C, 26.2; H, 0.5; N, 3.0.

Synthesis of {2-(CF₃CO)-C₄H₃N}Re(CO)₃(PPh₃) (2b**).** A solution of **1b** (0.101 g, 0.219 mmol) in 20 mL of hexane was treated with PPh₃ (0.060 g, 0.230 mmol) and refluxed for 1 h under an atmosphere of argon. Upon cooling to room temperature, formation of a yellow precipitate was observed. The solution was reduced to a third of the volume, further cooled in a freezer overnight, and filtered to give a yellow-orange product (0.103 g, 68%). IR data in CH₂Cl₂ (ν_{CO}): 1582 (m), 1905 (s), 1936 (s), 2032 (s). NMR data in CDCl₃: ¹H δ 6.34 (d, *J* = 4.4 Hz, 1 H), 7.01 (m, 1 H), 7.20 (m, 6 H, H_o), 7.30 (m, 1 H), 7.33 (t, *J* = 8.3 Hz, 6 H, H_m), 7.41 (t, *J* = 7.3 Hz, 3 H, H_p); ³¹P δ 20.16; ¹³C{¹H} δ 117.9 (q, ¹J_{CF} = 280 Hz, 1 C, CF₃), 120.6, 126.1, 128.6 (d, *J*_{CP} = 10 Hz, 6 C, C₆H₅), 129.3 (d, *J*_{CP} = 44 Hz, 3 C, C₆H₅), 130.5 (d, *J*_{CP} = 2 Hz, 3 C, C₆H₅), 133.5 (d, *J*_{CP} = 11 Hz, 6 C, C₆H₅), 139.0, 150.0, 170.5 (q, ²J_{CF} = 37 Hz, 1 C, C=O), 187.6 (d, *J*_{CP} = 69 Hz, 1 C, CO), 195.7 (d, *J*_{CP} = 67 Hz, 1 C, CO), 195.8 (d, *J*_{CP} = 67 Hz, 1 C, CO). Anal. Calcd for C₂₇H₁₈F₃N₁O₄P₁Re₁: C, 46.7; H, 2.6; N, 2.0. Found: C, 46.6; H, 2.5; N, 2.0.

Synthesis of {2-(CHO)-C₄H₃N}Re(CO)₃(pyridine) (3a**).** A solution of **1a** (0.390 g, 0.99 mmol) in 50 mL of hexane was treated with pyridine (0.1 mL, 1.24 mmol) and refluxed for 2 h under an atmosphere of argon. Upon cooling to room temperature, formation of a yellow precipitate was observed. The solution was further cooled in a freezer overnight and filtered to give a yellow product (0.410 g, 93%). IR data in CH₂Cl₂ (ν_{CO}): 1570 (m), 1906 (s), 1927 (s), 2030 (s). NMR data in CDCl₃: ¹H δ 6.42 (dd, *J* = 4.1 and 1.4 Hz, 1 H), 7.08 (dd, *J* = 4.1 and 0.9 Hz, 1 H), 7.28 (m, 2 H, pyridine), 7.64 (d, *J* = 1.4 Hz, 1 H), 7.77 (tt, *J* = 7.7 and 1.7 Hz, 1 H, pyridine), 8.38 (m, 2 H, pyridine), 8.73 (d, *J* = 1.4 Hz, 1 H, CHO); ¹³C{¹H} δ 118.1, 124.4, 125.4 (s, 2 C, pyridine), 138.3 (s, 1 C, pyridine), 144.3, 145.0, 152.0 (s, 2 C, pyridine), 181.2 (s, 1 C, CHO), 193.1 (s, 1 C, CO), 197.3 (s, 1 C, CO), 197.6 (s, 1 C, CO). Anal. Calcd for C₁₃H₉N₂O₄Re: C, 35.2; H, 2.1; N, 6.3. Found: C, 35.2; H, 2.0; N, 6.4.

X-ray Crystal Structure Analyses. Single crystals of **2b** and **3a** were obtained by the slow evaporation of a hexane solution. A Leica MZ7.5 stereomicroscope was used to identify suitable crystals of the same habit. Each crystal was coated in paratone, affixed to a Nylon loop, and placed under streaming nitrogen (110 K) in a SMART Apex CCD diffractometer (see details in the CIF files). The space groups were determined on the basis of systematic absences and intensity statistics. The structures were solved by direct methods and refined by full-matrix least squares on *F*². Anisotropic displacement parameters were determined for all non-hydrogen atoms. Hydrogen atoms were placed at idealized positions and refined with fixed isotropic displacement parameters. The following is a list of programs used: data collection and cell refinement, *APEX2*;¹² data reductions, *SAINTPLUS*, version 6.63;¹³ absorption correction, *SADABS*;¹⁴ structural solutions, *SHELXS-97*;¹⁵ structural refinement, *SHELXL-97*;¹⁶ graphics and publication materials, *SHELXTL*.¹⁷

c. DFT Calculations. All calculations were performed in the development version of the *Gaussian* suite of programs¹⁸ using DFT. Geometries were optimized using the ω B97XD¹⁹ functional, which includes different fractions of exact exchange in the long and short ranges, as well as a dispersion correction. All atoms were described with the def2-TZVPP basis set,²⁰ which describes the core electrons of the heavy atom (rhenium) using an effective core potential. The computed geometries were confirmed to be ground-state structures or transition states according to their number of imaginary frequencies. The enthalpies or free energies were computed at 298.15 K and 1 atm and are expressed in kcal/mol. Figures of computed geometries included in this work were rendered using *CYLview*.²¹

RESULTS AND DISCUSSION

a. 1a + PPh₃. The thermal reaction of **1a** with PPh₃ results in the spectral changes shown in Figure 1. The CO stretching bands of **1a** at 2112, 2010, 1993, and 1949 cm⁻¹ and the aldehyde absorbance at 1571 cm⁻¹ exhibit a first-order exponential decrease in intensity and are consistent with

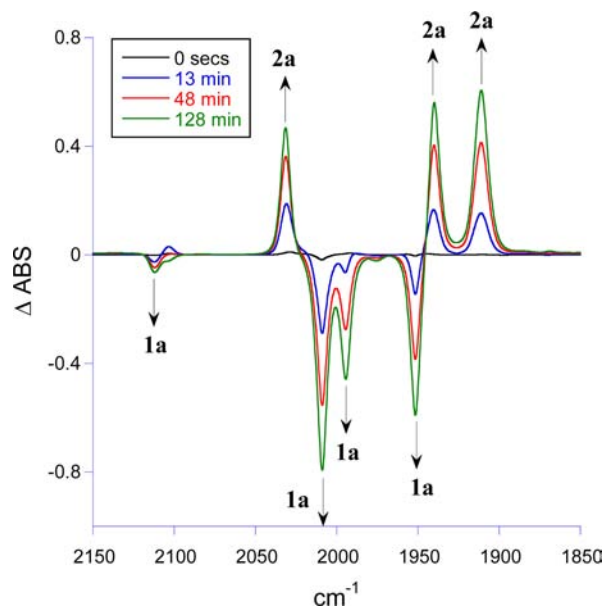


Figure 1. Difference FTIR spectra observed as a function of time upon reaction of a 3 mM solution of **1a** with 0.17 M PPh₃ in heptane at 303 K. The positive peaks are due to the growth of the product complex, **2a**, while the negative peaks are due to the disappearance of the reactant, **1a**.

literature values;⁹ product peaks due to **2a** at 2032, 1939, 1912, and 1580 cm⁻¹ increase at the same rate. The locations of the relevant IR bands are presented in Table 1. The observation of three CO stretching absorptions in the product complex is consistent with the previously determined crystal structure of {2-(CH₃CHO)C₄H₃N}Re(CO)₃PPh₃.⁹ While the CO ligands have local C_{3v} symmetry, a reduction in the symmetry due to the pyrrolyl ligand results in the splitting of the E band, yielding absorptions at 1939 and 1912 cm⁻¹ (see Table 1). The facial geometry of **2a** indicates loss of a CO ligand that is cis to both coordinating atoms of the bidentate pyrrolyl ligand and, as discussed previously,⁹ is consistent with the mutual trans influence of the CO ligands.

As shown in Figure 2, within the first few minutes of the reaction, additional peaks are observed to first increase rapidly and then decrease in intensity during the course of the reaction at 303 K. The complex associated with these absorptions (**IM**) exhibits the temporal profile shown in Figure 3. The reactant species **1a** also has a biexponential time profile with fast and slow components that match, within a factor of 2, the fast growth and slower decay of **IM**. These observations suggest the presence of an intermediate species along the **1a** → **2a** reaction

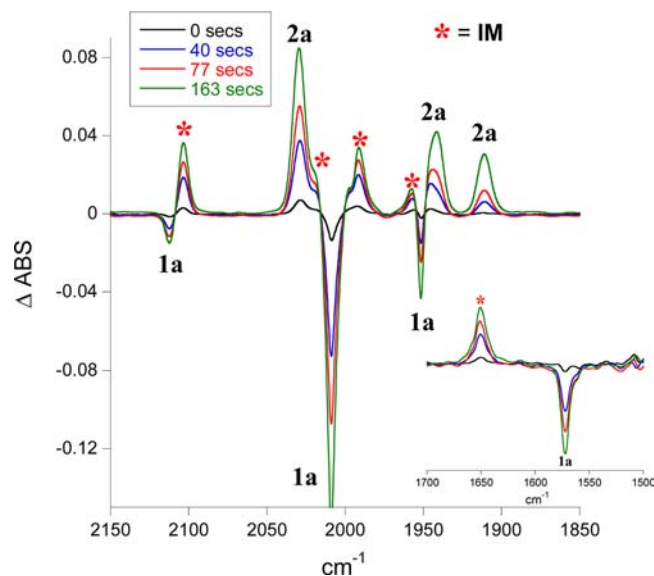


Figure 2. Difference FTIR spectra obtained at the start of the reaction between a 3 mM solution of **1a** and 0.17 M PPh₃ at 303 K in heptane. The peaks marked with **IM** are due to the formation of an intermediate species that grows rapidly and then decays over the course of the reaction at the same rate as the growth of the product complex **2a**. The inset shows spectral changes in the 1700–1500 cm⁻¹ region due to the C=O stretching of the aldehyde.

pathway. As discussed later, DFT calculations also confirm the viability of an intermediate complex along the CO displacement channel.

Four CO stretching bands are observed for **IM** at 2103, 2019, 1990, and 1957 cm⁻¹, confirming that generation of this intermediate does not require the displacement of a CO ligand from **1a**. Furthermore, the peak at 1651 cm⁻¹ associated with this complex is in good agreement with the C=O stretching band of the uncoordinated acetylpyrrolyl ligand observed at 1650 cm⁻¹. Put together, these data suggest that the incoming PPh₃ ligand initially displaces the weakly coordinated aldehyde group of the pyrrolyl ligand to generate an intermediate with the following structure:

This intermediate complex then proceeds to form the final product **2a** by loss of a CO molecule that must be cis to both the phosphine and N-coordinated pyrrolyl ligands, followed by recoordination of the aldehyde oxygen to the rhenium center. The overall reaction then appears to follow a **1a** → **IM** → **2a** pathway.

To determine whether **IM** is formed reversibly from **1a**, a heptane solution of **1a** and 0.4 M PPh₃ was allowed to react at

Table 1. Listing of All Relevant IR Absorptions, Experimental and Calculated, for the Complexes Studied

complex	ν (cm ⁻¹)	
	experimental (heptanes)	calculated (scaled) ^a
1a	2112, 2100, 1993, 1949, 1571	2110, 2015, 1996, 1955, 1561
1b	2115, 2014, 2001, 1958, 1583	
IM (PPh ₃)	2103, 2019, 1990, 1957, 1651	
IM (pyridine)	2106, 2015, 1982, 1945, 1650	2101, 2012, 1985, 1946, 1655
2a	2032, 1939, 1912, 1580	
2b	2035, 1946, 1917, 1582	
3a	2028, 1926, 1908, 1569	2023, 1934, 1918, 1559

^aCalculated values were scaled by a factor of 0.947 (see the text).

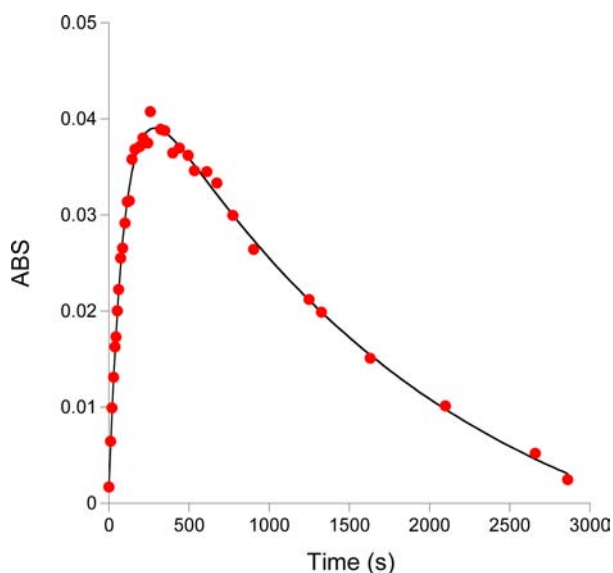
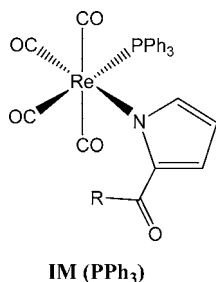


Figure 3. Temporal profile of the intermediate complex, **IM**, monitored at 2103 cm^{-1} obtained upon reaction of a heptane solution of **1a** with 0.17 M PPh_3 at 303 K . The time dependence of this species demonstrates a fast rise followed by a slower decay. The solid black line represents a biexponential fit to the data.



room temperature for a few minutes and the solution quenched at 263 K . Evaporation of the solvent yielded an amorphous yellow powder together with large white PPh_3 crystals. After hand separation of the PPh_3 crystals, the yellow powder was redissolved in heptane and spectra were acquired at 298 K over a 30-min time period. As shown in Figure 4, the initial spectrum clearly shows the presence of all three complexes, **1a**, **IM**, and **2a**. Under these conditions, **IM** converts completely to the reactant **1a** and there is no change in the concentration of **2a**. The data are therefore consistent with the reversible formation of **IM** from **1a**, with the equilibrium condition favoring the reactant complex. Furthermore, because conversion of **IM** to **2a** is not observed under these conditions, the overall CO displacement mechanism is consistent with a preequilibrium process with the $\text{IM} \rightarrow \text{1a}$ reaction barrier lower than that for $\text{IM} \rightarrow \text{2a}$. The overall data therefore suggest the reaction mechanism shown in Scheme 2.

The reaction of **1b** with $\text{L} = \text{PPh}_3$ was also studied to ascertain the effect of the electron-withdrawing CF_3 group upon the reaction rate and stability of the intermediate. As shown in Figure 5, the rate of CO displacement from **1b** is almost 6 times faster than that from **1a**. The available data do not allow for the origin of this rate enhancement to be determined with certainty. It is possible that the faster rate is due to a shift in the equilibrium toward **IM** as a result of weaker $\text{Re}-\text{O}$ binding in **1b** or because of differences in the stability of the transition state connecting **IM** to the product complex. This

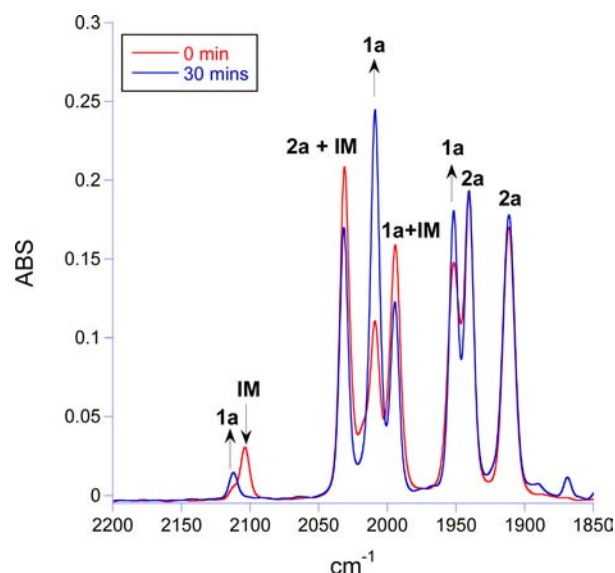


Figure 4. Spectral changes observed when a heptane solution initially containing **1a**, **IM**, and **2a** is left standing at 298 K . The spectra are consistent with the complete conversion of **IM** to the reactant **1a** while the concentration of **2a** is left unchanged. Because of the overlap between the CO bands of the various species, conversion is best observed at 2103 cm^{-1} (**IM**) and 2112 cm^{-1} (**1a**). The intensities of the product bands at 1939 and 1912 cm^{-1} due to **2a** are unchanged.

issue is discussed later in light of the DFT calculations. During the course of these studies, **2b** was isolated and a crystal structure obtained (Figure 6). The structure of this species is very similar to that of the previously characterized $\{2\text{-}(\text{CH}_3\text{CHO})\text{C}_4\text{H}_3\text{N}\}\text{Re}(\text{CO})_3\text{PPh}_3$ complex.

b. 1a + Pyridine. A complete kinetic analysis over a wide range of incoming ligand concentrations could not be performed with PPh_3 due to solubility limitations. Thus, pyridine was chosen as the displacing ligand for these experiments. As in the case of PPh_3 , the reaction of **1a** with pyridine results in complete conversion to the pyridine complex **3a** (Figure 7), which was isolated and a crystal structure obtained (Figure 8). The CO ligands are facially coordinated as in **2b**, and this geometry is consistent with the cis displacement of CO from **1a**. At early reaction times, an intermediate complex is observed with the same spectral features as those observed with PPh_3 , although it is significantly less stable and is observable for only a few minutes at 303 K . In an effort to obtain better spectroscopic evidence for this intermediate, the reaction was conducted at 286 K with $[\text{pyridine}] = 0.4\text{ M}$, and as shown in Figure 9, this species absorbing at 2106 , 2015 , 1982 , 1945 , and 1650 cm^{-1} is clearly observed for several seconds. As with the PPh_3 ligand, a 6-fold rate enhancement is observed when pyridine is used to displace CO from the CF_3 analogue (**1b**).

As discussed earlier, the kinetic data are consistent with a preequilibrium between **1a** and **IM** followed by slower conversion to the product complex (Scheme 2). Application of the preequilibrium assumption yields the dependence of k_{obs} on $[\text{pyridine}]$ shown in eq 1.

$$k_{\text{obs}} = \frac{K_{\text{eq}} k_2 [\text{pyridine}]}{1 + K_{\text{eq}} [\text{pyridine}]} \left(K_{\text{eq}} = \frac{k_1}{k_{-1}} \right) \quad (1)$$

A plot of k_{obs} versus $[\text{pyridine}]$ is therefore expected to demonstrate saturation behavior as the $[\text{pyridine}]$ becomes

Scheme 2

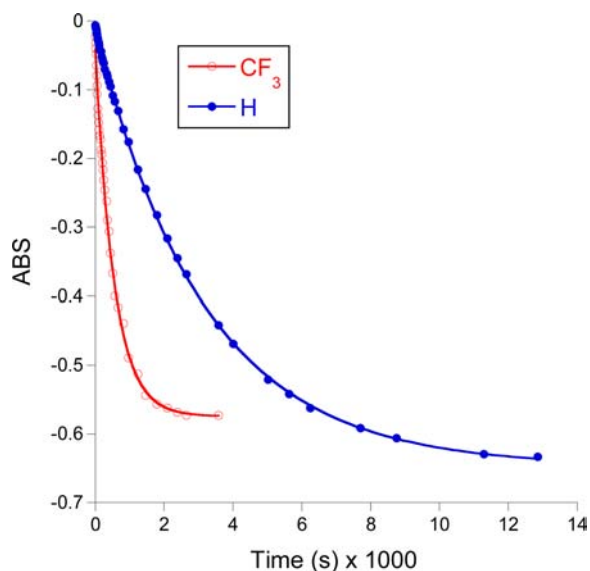
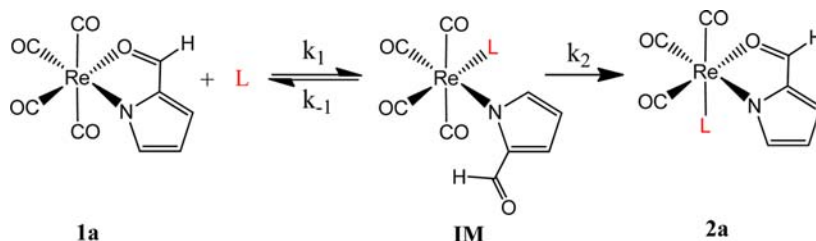


Figure 5. Plot of Abs versus time for the reaction of **1a** and **1b** with PPh_3 monitored at 2010 and 2001 cm^{-1} , respectively. A heptane solution of **1a** or **1b** was reacted with 0.17 M PPh_3 at 303 K.

large enough to force the equilibrium toward the intermediate, at which point k_{obs} is limited by the rate constant for conversion of **IM** to the product (k_2). However, as shown in Figure 10a, the observed dependence of k_{obs} on $[\text{pyridine}]$ is linear, implying that $K_{\text{eq}} \ll 1$, so that even at the highest $[\text{pyridine}]$ (4.8 M) employed $K_{\text{eq}}[\text{pyridine}] < 1$. As mentioned earlier, the observation that the intermediate converts completely to **1a** indicates that K_{eq} is, in fact, less than 1. Under these conditions, eq 1 reduces to

$$k_{\text{obs}} = K_{\text{eq}}k_2[\text{pyridine}] \quad (2)$$

and a plot of k_{obs} versus $[\text{pyridine}]$ should be linear, as observed, with a slope of $K_{\text{eq}}k_2$. The relevant mechanistic parameters are listed in Table 2. Unfortunately, the kinetic data do not allow for an independent measurement of K_{eq} or k_2 but rather their product. Thus, the activation enthalpy from the Eyring analysis, ΔH_{total} , shown in Figure 10b, is expected to yield the sum of ΔH_{eq} and ΔH_2^\ddagger rather than individual values. As discussed below, the experimental value of 15.4 ± 0.4 kcal/mol is in good agreement with a theoretical estimate of 13.4 kcal/mol for $\Delta H_{\text{eq}} + \Delta H_2^\ddagger$. Similarly, $\Delta S_{\text{total}} = \Delta S_{\text{eq}} + \Delta S_2^\ddagger$ and is determined to have a value of -22.4 ± 1.2 eu. While ΔS_{eq} is expected to be negative and ΔS_2^\ddagger positive, the magnitude of the latter value depends on the structure of the transition state and may not be positive enough to counter the negative entropy change for the equilibrium step. Thus, the overall negative entropy is not unreasonable given the proposed mechanism.

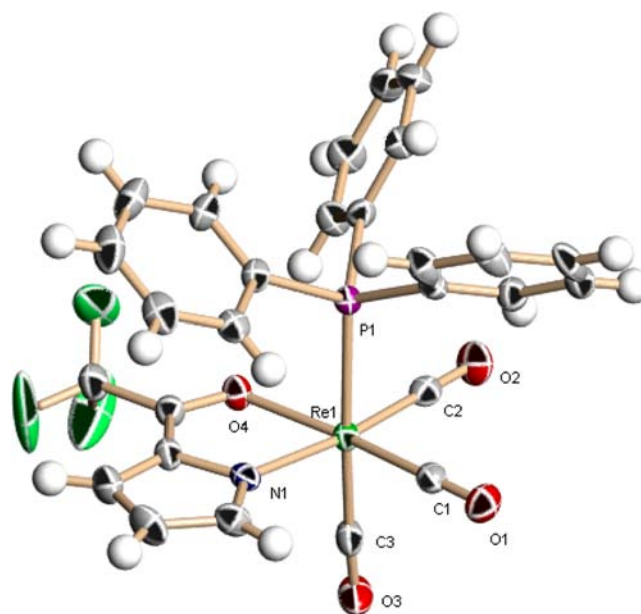


Figure 6. Crystal structure of **2b**. Selected bond lengths (Å) and angles (deg): $\text{Re1-C1} = 1.905(4)$, $\text{Re1-C2} = 1.918(4)$, $\text{Re1-C3} = 1.950(4)$, $\text{Re1-N1} = 2.152(3)$, $\text{Re1-O4} = 2.185(2)$, $\text{Re1-P1} = 2.4989(13)$; $\text{C1-Re1-C2} = 89.91(14)$, $\text{C1-Re1-C3} = 88.76(15)$, $\text{C2-Re1-C3} = 88.88(15)$, $\text{C1-Re1-N1} = 97.52(13)$, $\text{C2-Re1-N1} = 172.32(12)$, $\text{C3-Re1-N1} = 93.18(13)$, $\text{C1-Re1-O4} = 172.27(11)$, $\text{C2-Re1-O4} = 97.64(12)$, $\text{C3-Re1-O4} = 92.99(13)$, $\text{N1-Re1-O4} = 74.88(10)$, $\text{C1-Re1-P1} = 92.57(11)$, $\text{C2-Re1-P1} = 86.24(10)$, $\text{C3-Re1-P1} = 174.94(11)$, $\text{N1-Re1-P1} = 91.49(8)$, $\text{O4-Re1-P1} = 86.33(8)$.

To provide support for the experimental findings, detailed DFT calculations were performed. The energetic profile of the substitution reaction, together with the calculated spectroscopic properties of all of the species involved, was found to be in close agreement with the experimental values.

c. Theoretical Modeling. All calculations were performed using pyridine as the incoming ligand for comparison with the experimental results. To rule out the possibility of a dissociative mechanism of CO displacement in these systems, initial calculations focused on the determination of the CO binding enthalpy in **1a**. The calculated Re-CO bond dissociation energy (BDE) of 30.2 kcal/mol is considerably higher than the experimental activation enthalpy of 15.4 kcal/mol, supporting the experimental conclusion that the reaction does not occur by a dissociative but rather a lower-energy associative pathway. It should be noted, however, that the Re-CO bond is relatively weak, especially for a third-row metal. For example, in molecules such as $\text{Fe}(\text{CO})_5$ and $\text{M}(\text{CO})_6$ ($\text{M} = \text{Cr}, \text{Mo}, \text{W}$), the metal-carbonyl BDEs range from 37 to 46 kcal/mol,²² while in the thermally robust $\text{CpMn}(\text{CO})_3$ complex, the BDE is

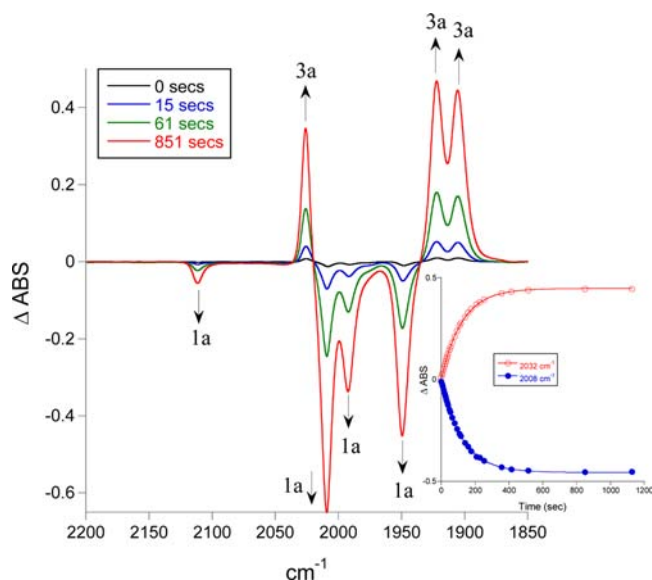


Figure 7. Difference FTIR spectra obtained at several time intervals upon reaction of **1a** with 1.6 M pyridine at 333 K. The inset shows the decay and growth of **1a** and **3a**, respectively.

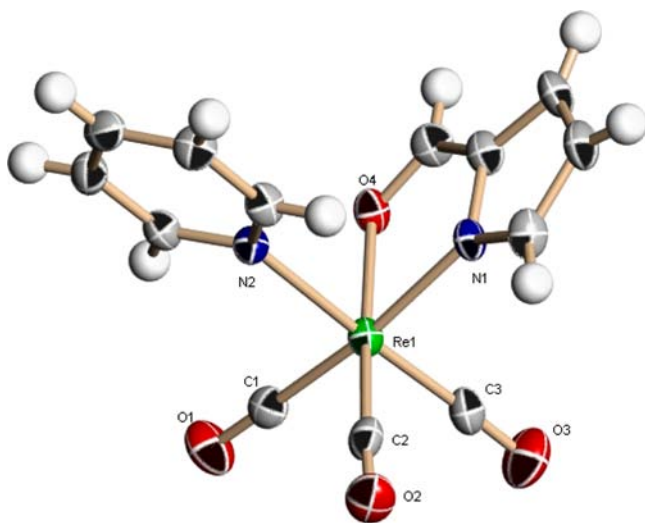


Figure 8. Molecular structure of **3a**. Selected bond lengths (Å) and angles (deg): Re1–C3 = 1.915(5), Re1–C2 = 1.916(5), Re1–C1 = 1.920(5), Re1–N1 = 2.140(4), Re1–O4 = 2.186(3), Re1–N2 = 2.227(4); C3–Re1–C2 = 87.3(2), C3–Re1–C1 = 89.4(2), C2–Re1–C1 = 91.3(2), C3–Re1–N1 = 92.85(19), C2–Re1–N1 = 98.00(19), C1–Re1–N1 = 170.56(17), C3–Re1–O4 = 95.14(19), C2–Re1–O4 = 173.71(16), C1–Re1–O4 = 94.55(17), N1–Re1–O4 = 76.12(14), C3–Re1–N2 = 177.25(17).

calculated to be >50 kcal/mol.²³ The calculations also indicate a higher free energy ($\Delta G^\ddagger = 28.1$ kcal/mol) for the direct displacement of CO by pyridine through an interchange pathway compared to the associative mechanism considered here.

The intermediate complex, with the structure suggested by the experimental data, was found to be a local minimum on the potential energy surface. Because the identities of **1a** and **3a** are known unambiguously, a comparison of the experimental vibrational values of these species with the calculated values results in a scaling factor of 0.9473. Application of this scaling factor to the calculated CO vibrational frequencies of the

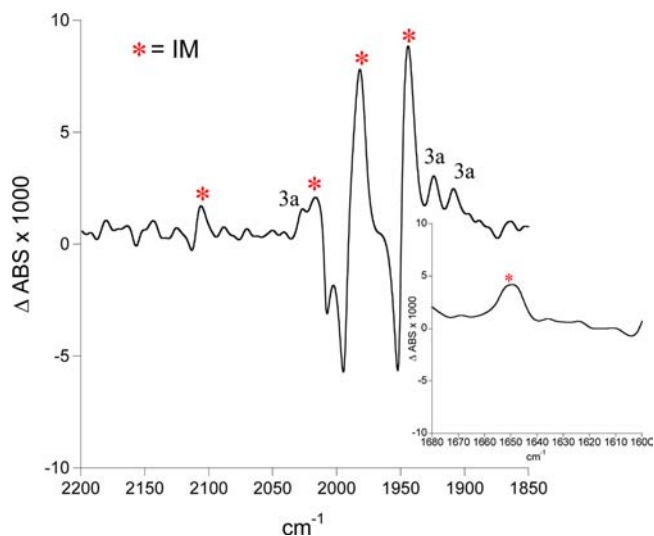


Figure 9. Difference FTIR spectra obtained immediately upon reaction of **1a** with 0.4 M pyridine at 286 K. The absorptions due to **IM** persist for less than 90 s under these conditions. The inset shows the aldehyde C=O stretch for **IM**, and its position at 1650 cm^{-1} is consistent with an uncoordinated oxygen atom.

intermediate complex yields estimates that are within 5 cm^{-1} of the observed values for **IM** (Table 1). The close agreement between the calculated and experimental vibrational values for this complex provides further confirmation for the correctness of its structural assignment. The calculated structures of **1a**, **IM**, and **3a** are shown in Figure 11. Interestingly, the Re–pyridine bond lengths are similar in both **IM** (2.255 Å) and **3a** (2.257 Å), indicating that this bond is already fully formed in the intermediate complex. The average Re–CO bond length for the CO fragments trans to the pyrrolyl ligand in **1a** is 1.935 Å, while it is calculated to be 2.015 Å for the *cis*-CO ligands. These bond lengths are consistent with the experimental finding of preferential *cis*-CO displacement and are indicative of a weaker Re–CO interaction in this case.

A reaction coordinate diagram (Figure 12) was obtained by calculating the lowest-energy path connecting the reactant, intermediate, and product complexes for both the **1a** → **3a** ($R = H$) and **1b** → **3b** ($R = \text{CF}_3$) reactions. A listing of all of the relevant thermodynamic parameters is presented in Table 3.

$R = H$. The product is found to be 2.2 kcal/mol more stable (ΔG°) than the reactant species. Relative to **1a**, the intermediate complex is calculated to be enthalpically favored by 7.3 kcal/mol but entropically disfavored, resulting in $\Delta G_{\text{eq}} = +4.7$ kcal/mol. As discussed earlier, the linearity of the k_{obs} versus [pyridine] plot suggests that $K_{\text{eq}} \ll 1$. The modeling results predict $K_{\text{eq}} \approx 4 \times 10^{-4}$ at 303 K and are therefore consistent with the kinetic data. The intermediate is found to lie in a well with the barrier for conversion to **1a** ≈ 4 kcal/mol lower than its reaction to **3a**, thereby justifying the validity of the pre-equilibrium assumption in the kinetic analysis. Another important agreement between theory and experiment comes from a comparison of the enthalpic parameters associated with the substitution reaction. The experimental estimate of $\Delta H_{\text{eq}} + \Delta H_2^\ddagger = 15.4$ kcal/mol is in good agreement with the predicted value of 13.4 kcal/mol. The structure of TS1 shows a significant lengthening of the Re–O bond, and the relatively low value of ΔH_1^\ddagger (9.1 kcal/mol) is consistent with the expected weak nature of this interaction (Figure 13). For the departing CO, the Re–CO bond length in TS1 is similar to that in the reactant

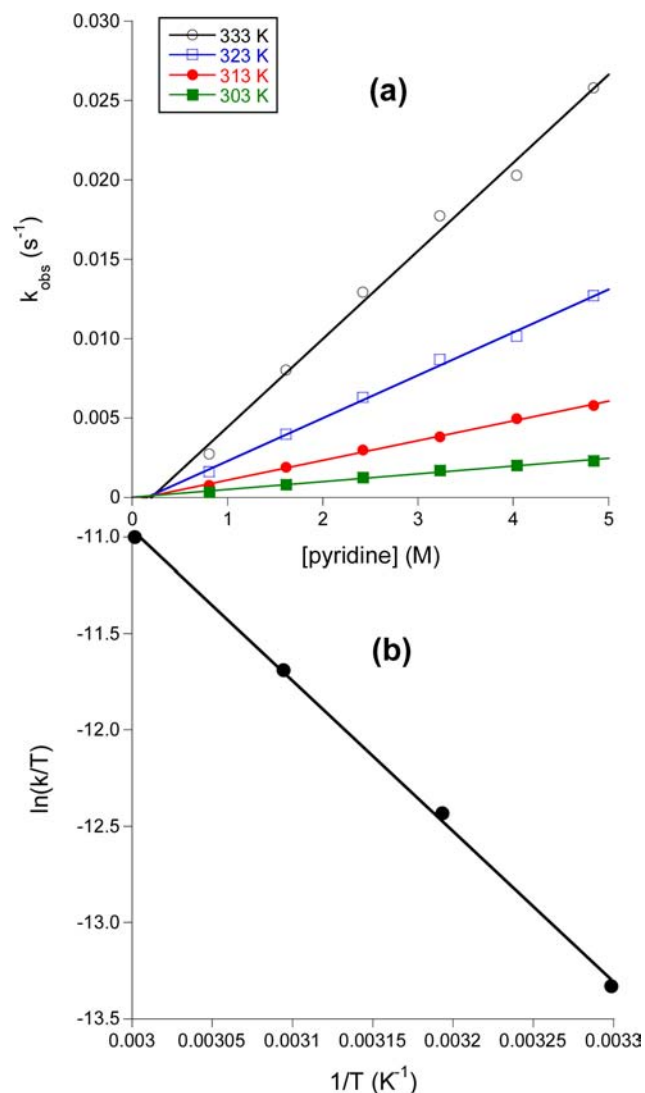


Figure 10. (a) Plot of k_{obs} versus [pyridine] at several temperatures for the reaction of **1a** with pyridine to form **3a**. (b) Eyring plot.

Table 2. Kinetic Parameters for the Reaction of **1a** with Pyridine at Several Temperatures

temperature (K)	$K_{\text{eq}}k_2$ (s^{-1}) $\times 1000$
303	0.49 ± 0.03
313	1.25 ± 0.03
323	2.71 ± 0.08
333	5.56 ± 0.24

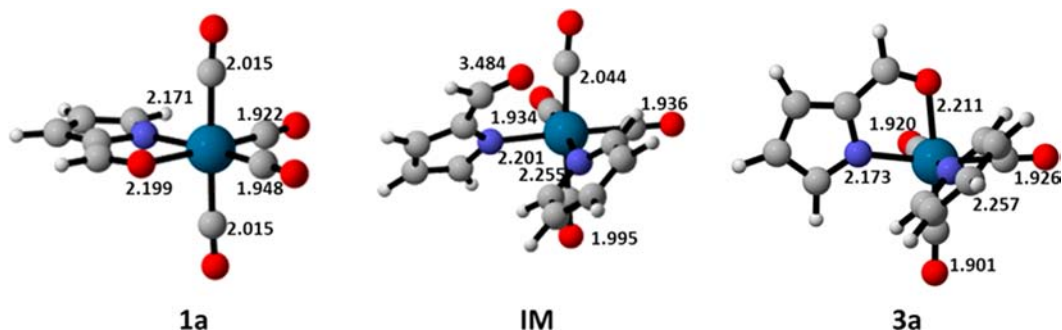


Figure 11. Calculated structures for **1a**, **IM**, and **3a**.

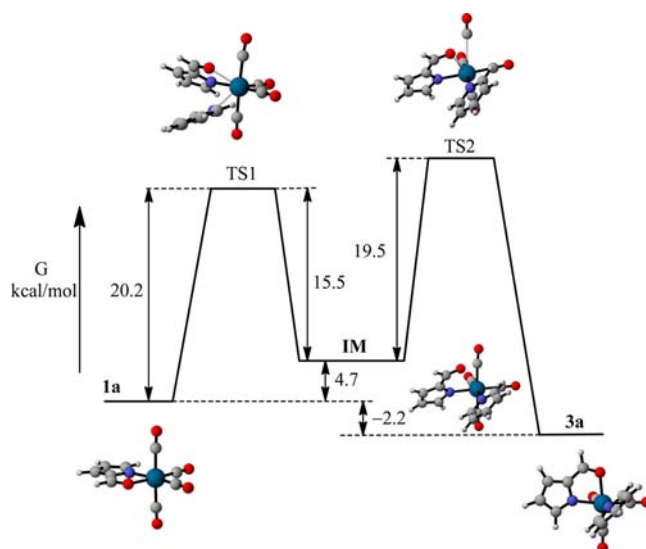


Figure 12. Reaction coordinate diagram for the reaction of **1a** with pyridine to form **3a** (R = H). The ΔG_{298}° values were obtained from the values listed in Table 3.

Table 3. Calculated Thermodynamic Parameters (kcal/mol) for the Relevant Species in the CO Displacement Reaction at 298.15 K

	R = H				
	1a	TS1	IM	TS2	3a
ΔG°	0	20.2	4.7	24.2	-2.2
ΔH°	0	9.1	-7.3	13.4	-4.1
	R = CF ₃				
	1b	TS1	IM	TS2	3b
ΔG°	0	17.3	2.3	20.8	-4.9
ΔH°	0	7.7	-8.1	12.1	-4.7

complex, indicating little disruption of this bond as the pyridine ligand approaches the metal center. The final step in the mechanism, k_2 , has the largest activation enthalpy ($\Delta H_2^\ddagger = 20.7$ kcal/mol), which is consistent with the disruption of the Re–CO interaction that is largely broken in **TS2**.²⁴ Nonetheless, because of the chelate effect, the slowest step in the mechanism is calculated to be the breaking of the Re–O bond ($\Delta G_1^\ddagger = 20.2$ kcal/mol) rather than dissociation of the more strongly bound CO ligand ($\Delta G_2^\ddagger = 19.5$ kcal/mol).

R = CF₃. The energetic profile for the reaction of **1b** with pyridine is similar to that for **1a**. The expected weaker Re–O interaction in **1b** due to the inductive effect of the CF₃ group is

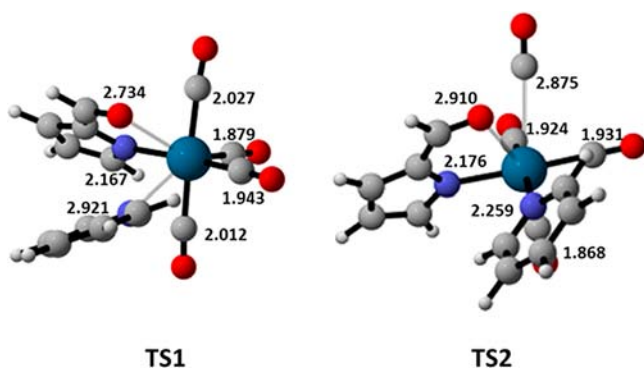


Figure 13. Calculated structures of the transition states in the reaction of **1a** with pyridine.

manifested in both a smaller activation barrier to TS1 ($\Delta H_1^\ddagger = 7.7$ vs 9.1 kcal/mol) and increased stability of the resulting intermediate ($\Delta H_{\text{eq}} = -8.1$ vs -7.3 kcal/mol) relative to the hydrogen analogue. As mentioned earlier, the product $K_{\text{eq}}k_2$, and hence the reaction rate, is almost 6 times larger for the displacement of CO from **1b** compared to **1a**. The calculations confirm this reactivity difference and indicate that, in the case of the CF_3 system, both a more stable intermediate (larger K_{eq}) and a lower barrier for its conversion to product (larger k_2) contribute to increased CO lability.

CONCLUSIONS

The thermal displacement of a CO molecule from a rhenium tetracarbonyl complex bearing a hemilabile pyrrolyl ligand by PPh_3 and pyridine has been investigated. As reported previously, the CO ligand is found to be unusually labile in this species, with the reaction complete within a few hours at room temperature. During early times in the reaction, an intermediate complex that is generated rapidly and then converts to the product tricarbonyl species is observed. This intermediate is identified as the $(\eta^1\text{-N-pyrrolylcarboxyaldehyde})\text{Re}(\text{CO})_4\text{L}$ ($\text{L} = \text{PPh}_3$ or pyridine) complex, which forms upon displacement of the aldehyde Re–O bond by the incoming ligand. This species then converts to the final complex by loss of a CO ligand. Theoretical modeling of the reaction using DFT confirms the presence of the intermediate complex along the reaction pathway, and the calculated energetic parameters agree well with the experimental values. While the Re–CO BDE is calculated to be 30.2 kcal/mol, the reaction proceeds with a 15.4 kcal/mol enthalpic barrier. It is postulated that the unusual lability of this complex is due to the presence of the weak aldehyde Re–O link that can easily dissociate to open a coordination site on the metal center and accommodate an incoming ligand prior to CO loss. This associative pathway provides a lower-energy reaction channel for the release of CO.

ASSOCIATED CONTENT

Supporting Information

CIF file giving X-ray structural data for **2b** and **3a** and a complete listing of all Cartesian coordinates for the modeled complexes. This material is available free of charge via the Internet at <http://pubs.acs.org>.

AUTHOR INFORMATION

Corresponding Author

*E-mail: djdarens@mail.chem.tamu.edu (D.J.D.), ashfaq.bengali@qatar.tamu.edu (A.A.B.).

Notes

The authors declare no competing financial interest.

ACKNOWLEDGMENTS

This publication was made possible by funding from the Qatar National Research Fund (member of Qatar Foundation). The experimental work was supported by NPRP Grant 09-157-1-024 and the theoretical studies by NPRP Grant 09-143-1-022.

REFERENCES

- (1) (a) Herrmann, W. A.; Cornils, B. *Applied Homogeneous Catalysis with Organometallic Compounds*; Wiley-VCH: Berlin, 2002. (b) Masters, C. *Homogeneous Transition-Metal Catalysis*; Chapman Hall: London, 1981. (c) Parshall, G. W.; Ittel, S. D. *Homogeneous Catalysis—The Application and Chemistry of Catalysis by Soluble Transition-Metal Complexes*; John Wiley and Sons: New York, 1980. (d) Cornils, B.; Herrmann, W. A. *J. Catal.* **2003**, *216*, 23.
- (2) (a) Johnson, T. R.; Mann, B. E.; Clark, J. E.; Foresti, R.; Green, C. J.; Motterlini, R. *Angew. Chem., Int. Ed.* **2003**, *43*, 3722. (b) Jaouen, G. *Bioorganometallics. Biomolecules, Labelling, Medicine*; Wiley-VCH: Weinheim, Germany, 2005.
- (3) (a) Ferber, B.; Tos, S.; Vessières, A.; Welter, R.; Jaouen, G. *Organometallics* **2006**, *25*, 5730. (b) Le Bideau, F.; Salmay, M.; Top, S.; Jaouen, G. *Chem.—Eur. J.* **2001**, *7*, 2289.
- (4) (a) Jaouen, G.; Vessières, A.; Butler, I. S. *Acc. Chem. Res.* **1993**, *26*, 361. (b) Jaouen, G.; Top, S.; Vessières, A.; Alberto, R. *J. Organomet. Chem.* **2000**, *600*, 23. (c) Salmay, M.; Vessières, A.; Brossier, P.; Butler, I. S.; Jaouen, G. *J. Immunol. Methods* **1992**, *148*, 65.
- (5) (a) Schmidt, K.; Jung, M.; Keilitz, R.; Schnurr, B.; Gust, R. *Inorg. Chim. Acta* **2000**, *306*, 6. (b) Jaouen, G.; Top, S.; Vessières, A.; Pigeon, P.; Leclercq, G.; Laios, I. *Chem. Commun.* **2001**, 383.
- (6) (a) Romao, C. C.; Blattler, W. A.; Seixas, J. D. *Chem. Soc. Rev.* **2012**, *41*, 3571. (b) Motterlini, R.; Otterbein, L. E. *Nat. Rev. Drug Discov.* **2010**, *9*, 728. (c) Alberto, R.; Motterlini, R. *Dalton Trans.* **2007**, 1651. (d) Motterlini, R.; Mann, B. E.; Johnson, T. R.; Clark, J. E.; Foresti, R.; Green, C. J. *Curr. Pharm. Des.* **2003**, *9*, 2525.
- (7) (a) Motterlini, R.; Clark, J. E.; Foresti, R.; Sarathchandra, P.; Mann, B. E.; Green, C. J. *Circ. Res.* **2002**, *90*, e17. (b) Clark, J. E.; Naughton, P.; Shurey, S.; Green, C. J.; Johnson, T. R.; Mann, B. E.; Foresti, R.; Motterlini, R. *Circ. Res.* **2003**, *93*, e2.
- (8) (a) Smith, H.; Mann, B. E.; Motterlini, R.; Poole, R. K. *IUBMB Life* **2011**, *63*, 363. (b) Nobre, L. S.; Al-Saharour, F.; Dopazo, J.; Saraiva, L. M. *Escherichia coli Microbiol.* **2009**, *155*, 813. (c) Nobre, L. S.; Seixas, J. D.; Romao, C. C.; Saraiva, L. M. *Antimicrob. Agents Chemother.* **2007**, *51*, 4303. (d) Davidge, K. S.; Sanguinetti, G.; Yee, C. H.; Cox, A. G.; McLeod, C. W.; Monk, C. E.; Mann, B. E.; Motterlini, R.; Poole, R. K. *J. Biol. Chem.* **2009**, *284*, 4516.
- (9) Mirebeau, J.-H.; Bideau, F. L.; Marrot, J.; Jaouen, G. *Organometallics* **2008**, *27*, 2911.
- (10) (a) Basolo, F. J. *Organomet. Chem.* **1990**, *383*, 579. (b) O'Connor, J. M.; Casey, C. P. *Chem. Rev.* **1987**, *87*, 307. (c) Jordan, R. B. *Reaction Mechanisms of Inorganic and Organometallic Systems*; Oxford University Press: New York, 1998; p 138. (d) Schuster-Woldan, H. G.; Basolo, F. J. *Am. Chem. Soc.* **1966**, *88*, 1657.
- (11) Son, S. U.; Paik, S.-J.; Lee, I. S.; Lee, Y.-A.; Chung, Y. K.; Seok, W. K.; Lee, H. N. *Organometallics* **1999**, *18*, 4114.
- (12) APEX2, version 2009.7-0; Bruker AXS, Inc.: Madison, WI, 2007.
- (13) SAINTPLUS: Program for Reduction of Area Detector Data 1034, version 6.63; Bruker AXS Inc.: Madison, WI, 2007.
- (14) Sheldrick, G. M. SADABS: Program for Absorption Correction of 1036 Area Detector Frames; Bruker AXS Inc.: Madison, WI, 2001.

(15) Sheldrick, G. M. *SHELXS-97: Program for Crystal Structure 1038 Solution*; Universität Göttingen: Göttingen, Germany, 1997.

(16) Sheldrick, G. M. *SHELXL-97: Program for Crystal Structure 1040 Refinement*; Universität Göttingen: Göttingen, Germany, 1997.

(17) Sheldrick, G. M. *SHELXL*, version 6.10; AXS Inc.: Madison, WI, 2000.

(18) Frisch, M. J.; Trucks, G. W.; Schlegel, H. B.; Scuseria, G. E.; Robb, M. A.; Cheeseman, J. R.; Scalmani, G.; Barone, V.; Mennucci, B.; Petersson, G. A.; Nakatsuji, H.; Caricato, M.; Li, X.; Hratchian, H. P.; Izmaylov, A. F.; Bloino, J.; Zheng, G.; Sonnenberg, J. L.; Hada, M.; Ehara, M.; Toyota, K.; Fukuda, R.; Hasegawa, J.; Ishida, M.; Nakajima, T.; Honda, Y.; Kitao, O.; Nakai, H.; Vreven, T.; Montgomery, J. A., Jr.; Peralta, J. E.; Ogliaro, F.; Bearpark, M.; Heyd, J. J.; Brothers, E.; Kudin, K. N.; Staroverov, V. N.; Kobayashi, R.; Normand, J.; Raghavachari, K.; Rendell, A.; Burant, J. C.; Iyengar, S. S.; Tomasi, J.; Cossi, M.; Rega, N.; Millam, J. M.; Klene, M.; Knox, J. E.; Cross, J. B.; Bakken, V.; Adamo, C.; Jaramillo, J.; Gomperts, R.; Stratmann, R. E.; Yazyev, O.; Austin, A. J.; Cammi, R.; Pomelli, C.; Ochterski, J. W.; Martin, R. L.; Morokuma, K.; Zakrzewski, V. G.; Voth, G. A.; Salvador, P.; Dannenberg, J. J.; Dapprich, S.; Parandekar, P. V.; Mayhall, N. J.; Daniels, A. D.; Farkas, O.; Foresman, J. B.; Ortiz, J. V.; Cioslowski, J.; Fox, D. J. *Gaussian Development Version*, revision H.13; Gaussian, Inc.: Wallingford, CT, 2009.

(19) Chai, J.-D.; Head-Gordon, M. *Phys. Chem. Chem. Phys.* **2008**, *10*, 6615–6620.

(20) Weigend, F.; Ahlrichs, R. *Phys. Chem. Chem. Phys.* **2005**, *7*, 3297–3305.

(21) Legault, C. Y. *CYLview*, 1.0b; Université de Sherbrooke: Sherbrooke, Quebec, Canada, 2009; <http://www.cylview.org>.

(22) Lewis, K. E.; Golden, D. M.; Smith, G. P. *J. Am. Chem. Soc.* **1984**, *106*, 3905.

(23) (a) Swennenhuis, B. H. G.; Poland, R.; Fan, W. Y.; Darensbourg, D. J.; Bengali, A. A. *Organometallics* **2010**, *49*, 7597.

(b) Davies, K. W.; Maivald, D.; Grabowski, J. J. *J. Photochem. Photobiol. A* **2008**, *197*, 335.

(24) The distance between the departing CO and the metal center in TS2 is 2.875 Å, significantly longer than the average Re–CO bond distances of 1.975 Å and 1.916 Å in the reactant and product, respectively.